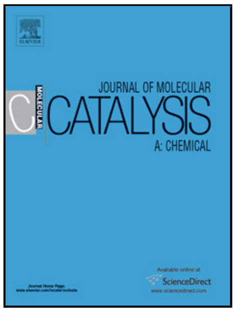

Title: CaO–ZrO_2 nanocomposite oxide prepared by urea hydrolysis method as heterogeneous base catalyst for synthesis of chromene analogues

Author: Sagnika Pradhan Vivekananda Sahu B.G. Mishra

PII: S1381-1169(16)30454-X
DOI: http://dx.doi.org/doi:10.1016/j.molcata.2016.10.031
Reference: MOLCAA 10093

To appear in: *Journal of Molecular Catalysis A: Chemical*

Received date: 9-6-2016
Revised date: 26-10-2016
Accepted date: 28-10-2016

Please cite this article as: Sagnika Pradhan, Vivekananda Sahu, B.G.Mishra, CaO–ZrO2 nanocomposite oxide prepared by urea hydrolysis method as heterogeneous base catalyst for synthesis of chromene analogues, Journal of Molecular Catalysis A: Chemical http://dx.doi.org/10.1016/j.molcata.2016.10.031

<AT>CaO-ZrO$_2$ nanocomposite oxide prepared by urea hydrolysis method as heterogeneous base catalyst for synthesis of chromene analogues

<AU>Sagnika Pradhan, Vivekananda Sahu, B.G. Mishra*
##Email##brajam@nitrkl.ac.in##/Email##
<AU>
<AFF>Department of Chemistry, National Institute of Technology, Rourkela-769008, Odisha, India

<PA>*Corrresponding author.

<ABS-Head><ABS-HEAD>Graphical abstract
<ABS-P>
<ABS-P><xps:span class="xps_Image">fx1</xps:span>

<ABS-HEAD>Highlights► CaO-ZrO$_2$ nanocomposite oxides prepared by urea hydrolysis method ► The Ca^{2+} substitute for Zr^{4+} to form a solid solution in a limited composition range ► Creation of new basic sites of higher strength due to Ca^{2+} incorporation to ZrO$_2$ ► Presence of O^{2-} vacancy and distortion in oxygen sublattice due to Ca^{2+} incorporation ► The CaO-ZrO$_2$ composite highly efficient catalyst for synthesis of chromene analogues

<ABS-HEAD>Abstract

<ABS-P>A series of CaO-ZrO$_2$ nanocomposite oxides containing 2-50 mol% of CaO were synthesized employing urea as a mild hydrolyzing agent. The nanocomposite systems were characterized using XRD, Fourier analysis, TPD, Raman, XPS, TGA-DSC, FESEM, HRTEM, and BET surface area measurement techniques. XRD study indicated selective stabilization of the tetragonal zirconia phase in the composite oxide. Upto 20 mol% CaO, the Ca^{2+} ions substituted for Zr^{4+} ions in the zirconia lattice to form a substitutional solid solution. Beyond 20 mol% CaO, the presence of a mixed phase system consisting of the solid solution phase, CaO and nonstoichiometric Zr$_{0.93}$O$_2$ phase was observed. The composite oxides contain crystallites with size <20 nm as observed from Fourier and HRTEM analysis. TPD study revealed a significant enhancement in the basicity of zirconia as a result of Ca^{2+} incorporation. XPS study confirmed presence of different lattice oxygen as potential basic sites. Raman spectral data indicated the presence of oxygen vacancy and distortion in oxygen sublattice due to Ca^{2+} incorporation to zirconia. Microscopic investigation of the composite oxide suggested a gradual morphological change from rod shape particles to flake like and subsequently to cubic morphology with increase in CaO content in the composite. The CaO-ZrO$_2$ nanocomposite oxides were used as an efficient and recyclable heterogeneous base catalyst for synthesis of chromene analogues. Structurally diverse 2-amino-4H-chromenes and 2-amino-2-chromenes were synthesized in high yield and purity under mild condition using CaO-ZrO$_2$ material as catalyst and multicomponent condensation approach.

<KWD>Keywords: 4H-chromene; 2-amino-2-chromene; CaO-ZrO$_2$; Raman; Urea hydrolysis

---

<H1>1. Introduction

Catalytic application of novel heterogeneous base catalyst in fine chemical synthesis is a promising field of research with potential application in pharmaceuticals and related fine chemical industries [1-5]. Among different heterogeneous base catalysts used in fine chemical synthesis, the alkali and alkaline earth metal oxides are quite promising because they are inexpensive, easy to prepare and display strong surface basic sites capable of promoting a variety of base catalyzed reactions [1-3]. However, the low surface area and deactivation of these oxide materials by surface passivation are important factors which influence their catalytic activity. In recent years, there is significant effort to design novel heterogeneous base catalyst with high surface area, structural stability and molecularly defined basic sites. The mesoporous hybrid material containing organic basic moieties tethered to the internal surface are the most widely investigated new generation base catalyst [6]. Recently, the surface and structural modification of zirconia using alkali and alkaline earth metal ions such as Cs^+, Na+, Ca^{2+} and Mg^{2+} ions has been actively pursued to generate thermally robust high surface area heterogeneous base catalyst with strong surface basicity [7-14]. For example, hard templating approach has been used to prepare sodium incorporated mesoporous zirconia with thermally stable tetragonal crystalline frameworks and superbasicity (27.0 in Hammet scale). The sodium modified mesoporous tetragonal zirconia exhibit excellent catalytic activity for synthesis of dimethyl carbonate [7]. The exchange of surface –OH group of hydrous zirconia with Cs^+ ions have been carried out to prepare a novel class of heterogeneous base catalyst. The Cs modified zirconia nanoparticles exhibit enhanced surface basicity and activity for transesterification of vegetable oil compared to alkaline earth metal oxides and LDH materials [8]. The incorporation of Ca^{2+} ions into the zirconia lattice to generate strong surface basic function has been a subject of intense study in literature [11-18]. The CaO forms a substitutional solid solution with ZrO_2 [13,15,18]. The incorporation of Ca^{2+} ions into the ZrO_2 lattice increases the iconicity of the crystal [11,13,15]. The nonstoichiometric solid solution phase exhibit strong surface basicity, high thermal stability and stable active sites for base catalyzed reactions. The CaO-ZrO_2 mixed oxide systems have been studied as catalyst for dehydration of 2,3-butanediol, synthesis of dimethyl carbonate and transesterification a variety of oils including waste cooking oil, refined rapeseed oil and soybean oil [11, 15-18]. The CaO-ZrO_2 mixed oxide system has also been used as efficient support for metallic nanoparticles for application as bifunctional catalysts [12, 19-22]. Ni Metal nanoparticles loaded on CaO-ZrO_2 has been studied extensively as catalyst for reforming reaction including dry reforming of methane and ethanol stem reforming [12, 19, 21]. The presence of Ca^{2+} ions in ZrO_2 lattice inhibits coke formation and enhances the stability and life time of the catalyst. Similarly, the Ru metal supported on CaO-ZrO_2 mixed oxide exhibit excellent catalytic activity for selective oxidation of alcohols with molecular oxygen [22]. The basicity of the CaO-ZrO_2 material can be tuned by adjusting the Ca/Zr ratio and proper choice of preparative method [15]. The reported studies suggest promising potential of CaO-ZrO_2 material for base catalyzed reactions. However, the applicability of this important catalytic material for base catalyzed fine chemical synthesis is yet to be explored. In order to explore the applicability of CaO-ZrO_2 material in the domain of fine chemical synthesis, in this work, we have prepared a series of CaO-ZrO_2 nanocomposite materials using urea hydrolysis method and studied their catalytic application for synthesis of a wide variety of biologically important chromene analogues.

The chromene moiety represents an important class of chemical units which are found in many natural products [23]. Chromene analogues particularly the 2-amino-2-chromenes and 2-amino-4H-chromene exhibit interesting pharmacological properties besides their use as value added products in chemical industries [23-27]. The 4H-chromene derivatives exhibit a wide spectrum of biological activities such as anticancer, anticoagulant, antibacterial, and fungicidal properties [27,28].The 2-amino-chromenes are widely employed as pigments, cosmetics and potential agrochemicals [23,4,5]. Due to the widespread application, the development of facile and clean protocol for synthesis of these compounds has been a subject of intense study in literature. The most efficient route for synthesis of 2-amino 4H-chromene involve the multicomponent condensation of aldehyde, malononitrile and 1,3-dicarbonyl compounds using basic catalyst [26,27]. Similarly, the 2-amino-2-chromenes are synthesized by base catalyzed multicomponent condensation (MCC) of aldehyde, malononitrile and α-naphthol [24,25]. Several homogeneous and heterogeneous catalytic systems including piperazine, Potassium phthalimide, tetrabutylammonium fluoride, I_2/K_2CO_3, basic ionic liquid, acid hydrolysate of tendons, Silica bonded N-propylpiperazine, amino functionalized silica gel, and DMAP (4-dimethylaminopyridine) functionalized polyacrylonitrile fiber catalyst have been used for the synthesis of these two classes of compounds [23-35]. However, most of the methods require longer time, stoichiometric reagents, and toxic solvents providing moderate to good yields of the product. Moreover, many procedures employ homogeneous catalyst and supported reagents which suffer from drawback such as recovery, recyclability, leaching and stability of the active sites. In our previous work, we have demonstrated the use of alkali and alkaline earth metal oxide based nanomaterials as catalyst for synthesis of 2-amino-2-chromene [4,5]. In continuation of our interest to develop zirconia based heterogeneous catalyst with strong acid-base property for application in organic synthesis [36-38], in this work, we have used CaO-ZrO_2 nanocomposite oxide as an efficient and recyclable heterogeneous catalyst for synthesis of 2-amino-4H-chromene and 2-amino-2-chromenes using MCC approach.

<H1>2. Experimental

Calcium nitrate ($Ca(NO_3)_2.4H_2O$), zirconyl chloride ($ZrOCl_2.8H_2O$) and urea (N_2H_4CO) were procured from Merk India Limited. All the reagents used in this study were of AR grade (> 99.9% purity) which were used directly in the experiments without further purification. Double distilled water prepared in the laboratory was used in composite oxide preparation.

<H2>2.1 Preparation of CaO (x mol%)-ZrO_2 nanocomposite oxides (xCa-Zr-O)

The xCa-Zr-O nanocomposite oxides containing different mol% CaO were prepared by hydrolysis and co-condensation of calcium nitrate and zirconyl chloride salt solution using urea as a mild hydrolyzing agent. Required amount of 0.5 M calcium nitrate and zirconyl chloride precursor salt solutions were mixed with equimolar quantity of urea solution. The resulting solution was refluxed for 12 h at 100°C. The obtained white precipitate was filtered and washed several times with hot water to remove the chloride ions ($AgNO_3$ test). The solid material was subsequently dried in a hot air oven at 120°C for 12 h and calcined at 700°C for 2 h to obtain the xCa-Zr-O nanocomposite oxides. The choice of the calcination temperature is based on earlier reports where the incorporation of Ca^{2+} ions into the zirconia lattice has been observed for calcination temperature in the range of 700-800°C [11, 14-16,18]. Moreover, at these calcination temperatures the evolution of strong basic sites has been noticed on CaO-ZrO_2 catalyst surface [15]. Using this procedure, xCa-Zr-O composite oxides containing x =2, 5, 10, 20, 50 mol% of CaO were prepared. The CaO(x mol%)–ZrO_2 nanocomposite materials were referred to as xCa-Zr-O in the subsequent text where x represents the mol% of CaO present in the composite oxide. The prepared catalytic materials were stored in a vacuum desiccator in air tight borosilicate glass container.

<H2>2.2 Characterization techniques

The XRD patterns of the pure ZrO_2, CaO and xCa-Zr-O nanocomposite oxides were recorded using a Rigaku Ultima IV multipurpose X-ray diffraction system. The XRD measurements were carried out in the 2θ range of 20–70° with a scan speed of 2 degrees per minute using CuKα (k = 1.5418Å) radiation. The specific surface area of the samples was determined by BET method using

N_2 adsorption/desorption at 77 K on a Quantachrome autosorb gas sorption system. The composite oxide samples were degassed at 150°C for 2 h prior to the sorptometric studies. FESEM pictures were taken using Nova Nano SEM/FEI microscope. The powder sample was placed on carbon tape followed by gold spitting for three minutes prior to the FESEM analysis. The TEM images of the 20Ca-Zr-O composite oxide was recorded using TECNAI 300kV equipment using carbon coated copper grids of 300 mesh size as substrate. The micro- Raman spectra were obtained on a Horiba Jobin-Yvon spectrometer using a 17 mW He–Ne laser light source (excitation wavelength 632.8 nm). The X-ray photoelectron spectra of 20Ca-Zr-O sample was recorded using SPECS make (Germany) spectrophotometer with 150 mm hemispherical analyzer at band pass energy of 12 eV. Monochromatic Al Kα radiation of 1486.74 eV was used as X-ray source. Binding energy corrections due to electrostatic charging was made relative to the C1s peak taken as 284.6 eV. Thermogravimetry analysis of the 20Ca-Zr-O and 50Ca-Zr-O composite oxides was performed using a Perkin- Elmer TGA-7 apparatus in air atmosphere (30 ml/min) with a linear heating rate (10°C/min) from room temperature to 600°C. The number of basic sites on the xCa-Zr-O composite oxides was estimated by CO_2 TPD experiments using Chembec 3000, Quantachrome instrument with a TCD detector. Prior to CO_2 adsorption, approximately 200 mg of the sample was degassed at 250°C under flowing He for 2 h. The sample was then allowed to cool to the room temperature under flowing He. The sample was exposed to flowing CO_2 gas (100%) for 1h, after which it is purged with He gas for 30 min to remove the excess physisorbed carbon dioxide molecules. The CO_2-TPD profiles were recorded by rising the temperature from 300 K to 923 K at a rate of 10 K min^{-1}. The ^{1}H NMR spectra were recorded with Bruker 400 MHz NMR spectrometer using TMS as internal standard.

<H2>2.3 Catalytic activity study

The catalytic activity of the xCa-Zr-O nanocomposite oxides was evaluated for the multicomponent one pot synthesis of 2-amino 4H-chromenes and 2-amino-2-chromenes. Prior to the catalytic tests, the xCa-Zr-O nanocomposite catalyst materials were pretreated by heating at 450°C for 2 h under flowing N_2 (40 ml/min) to remove any adsorbed CO_2 and H_2O species.

<H3>2.3.1 Synthesis of 2-amino 4H-chromenes

In a typical procedure, aromatic aldehyde (2 mmol), malononitrile (2 mmol), and dimedone (2 mmol) was dissolved in 3 ml of aqueous ethanol (1:1 ratio) to which 20Ca-Zr-O catalyst (50 mg) was added. The reaction mixture was stirred at 50°C for 1 h. The progress of the reaction was monitored by thin-layer chromatography (TLC). After completion of the reaction, as indicated by TLC, 05 ml of ethanol was added to the reaction mixture and it was filtered. The crude product was recovered from the ethanolic solution and recrystallized from hot methanol to afford the pure product.

<H3>2.3.2. Synthesis of 2-amino-2-chromenes

The synthesis of 2-amino-2-chromenes was carried out by multicomponent one pot condensation of aromatic aldehydes, malononitrile, and α-naphthol in presence of 20Ca-O-Zr catalyst. A 1:1 mixture of polyethylene glycol (PEG-400, average molecular mass: 380-420 g/mol) and water was used as solvent. In a typical procedure, reaction mixture containing benzaldehyde (2 mmol), malononitrile (2 mmol), α-naphthol (2 mmol) and 20Ca-Zr-O (50 mg) catalyst in PEG–water (3 ml; 1:1 mixture) was stirred at 50°C for 1h. Upon completion of the reaction as monitored by TLC, the reaction mixture was diluted with water (5 ml) and the obtained solid compound was removed by filtration. The reaction product was separated by dissolution in hot ethanol (5ml) followed by simple filtration to separate the catalyst. The crude product was recovered from the ethanolic solution and recrystallized to afford the pure product.

<H1>3. Results and discussion

<H2>3.1 Characterization of the xCa-Zr-O nanocomposite oxides

The XRD patterns of the xCa-Zr-O nanocomposite oxides along with pure ZrO_2 material are presented in Fig 1. Zirconia prepared by urea hydrolysis method exhibit intense and broad diffraction peaks with d spacing values of 3.12, 2.92, 2.82, 2.52, 2.19, 1.8, 1.65 and 1.53 Å. These peaks correspond to the presence of a mixture of monoclinic and tetragonal phases (Fig. 1a) (JCPDS-ICDD File no. 83-0940 and 81-1545). The percentage tetragonal phase in the zirconia sample is 58% calculated using the Toroya's method [38]. Addition of 2 mol% of CaO into the zirconia matrix results in selective stabilization of the tetragonal phase of zirconia. The 2Ca-Zr-O sample exhibit characteristic reflection from the tetragonal phase of zirconia. The tetragonal phase is preserved in all composite oxide materials. No new crystalline phase corresponding to either CaO or $CaZrO_3$ could be detected upto 20 mol% CaO content in the composite oxide system. In contrast to this observation, the 50Ca-Zr-O material, in addition to the characteristic *t*-ZrO_2 reflections, display less intense but well defined diffraction peaks with d spacing of 3.01, 2.27, 2.08, 1.90 and 1.87 Å. The peaks at 2.27, 2.08 and 1.87 Å corresponding to the presence of non-stoichiometric zirconia ($Zr_{0.93}O_2$) whereas the peaks at 3.01 and 1.90 Å correspond to the CaO phase (JCPDS-ICDD File no. 81-1319 and 74-1226). The tetragonal reflections shift gradually to lower 2θ value with increase in CaO content in the composite oxide (Fig. 2I). The cell parameters and cell volume are calculated using the software POWD. The plot of cell volume *vs* CaO content exhibits a liner relationship satisfying the Vegards Law (Fig. 2II). This observation indicates an expansion in the zirconia lattice as a result of substitution of Ca^{2+} (ionic radius =1.0 Å) for Zr^{4+} (Ionic radius =0.84 Å). The Ca^{2+} ion being larger in size is responsible for expansion of the zirconia lattice. The CaO-ZrO_2 composite oxide thus contains a substitutional solid solution and retains the tetragonal lattice of zirconia. The tetragonal phase of zirconia is known to be selectively stabilized in presence of aliovalent dopants in ZrO_2 lattice [38-40]. It has been observed that for an oversize dopant such as Ca^{2+} the oxygen vacancy resides near the Zr^{4+} ions [39,40]. The selective stabilization of the tetragonal phase in is study can be ascribed to the presence of oxygen vacancy which prevents the phase transformation of tetragonal phase by blocking the dislocation motion. The XRD study indicate that upto 20Ca-Zr-O the composite oxide material contain a solid solution phase whereas the 50Ca-O-Zr material is a mixed phase system consisting of the solid solution phase, a cation deficient nonstoichiometric zirconia phase and CaO.

The microstructural characteristics of the xCa-Zr-O materials is studied using Fourier line profile analysis of the broadened XRD patterns by Warren and Averbach method [41] using the software BRAEDTH [42]. The Fourier analysis is carried out by taking the ZrO_2 T (111) and T (220) peaks for all composite oxide samples. The plots of the volume weighed distribution function (PV) and size coefficient (AS) as a function of Fourier length are presented in Fig. 3I and II respectively. Pure ZrO_2 show a wide range of distribution function, the crystallite size distribution being extended beyond 40 nm. This observation suggests that the zirconia sample contain polycrystalline particles with larger average crystallite size. Contrary to this observation, the 2Ca-Zr-O, 5Ca-Zr-O, 10Ca-Zr-O and 20Ca-Zr-O composite materials exhibit a comparable narrow size distribution function (< 30 nm). The crystallite size and rms strain of the xCa-Zr-O material are calculated from the AS~L plot and are presented in Table 4. The calculated crystallite size data indicates that the xCa-Zr-O material upto 20 mol% CaO, contain smaller crystallites compared to ZrO_2 and

50Ca-Zr-O materials. The rms strain exhibit an inverse trend for the composites. The higher lattice strain observed in case of xCa-Zr-O composites is due to the presence of local and random lattice defects due to their smaller crystallite size.

In order to study the thermal transformation behavior, the TG-DSC analysis of the hydroxy precipitate is carried out in air atmosphere. The TG-DSC profiles of 10Ca-Zr-O and 50Ca-Zr-O material are resented in Fig. 4. The 10Ce-Zr-O material exhibit a major weight loss of 22 wt% in the temperature range of 50-250^{o}C. Two weight loss regions could be discerned in this temperature range due to removal of physisorbed and coordinated water molecules. Both the weight losses are endothermic in nature. At higher temperature, however, the weight loss is more gradual in the TG profile without any well-defined inflection point. The DSC curve of 10Ca-Zr-O material exhibit an exothermic peak in the temperature range of 500-550^{o}C. This peak can be assigned to the dehydration and dehydroxylation of the hydroxy precipitate to the corresponding 10Ce-Zr-O composite oxide. The TG profile of 50Ca-Zr-O material, on the other hand, shows three weight loss upto 350^{o}C. The weight loss below 150^{o}C is due to removal of physisorbed water whereas the high temperature loss accounts for the removal of different coordinated water molecules. Beyond this temperature, a gradual but significant weight loss is observed in the range 450-600^{o}C. In the DSC profile, this material exhibit three endothermic and two exothermic peaks. The DSC and TG profile of 50Ca-Zr-O precipitate precursor indicate that it is microscopically inhomogeneous leading to uneven distribution of both ions. The uneven distribution of the ions may lead to local segregation of the two hydroxide phases which transform to a multiphase oxide system in the temperature range of 450-600^{o}C. The TG analysis of 50Ca-Zr-O is supported by the XRD study where the presence of a mixed phase system consisting of the $Ca_xZr_{1-x}O_{2-x}$ solid solution, a cation deficient nonstoichiometric zirconia phase ($Zr_{0.93}O_2$) and pure CaO phase is observed.

The X-ray photoelectron spectra of the 20Ca-Zr-O material are presented in Fig. 5. The survey spectra in Fig. 5a display the characteristic spectral features due to the presence of Ca, Zr, C and O species in the composite material. In the Zr 3d spectral region, the 20Ca-Zr-O material exhibits a broad doublet with maxima at 182.0 eV and 184.2 eV. These peaks corresponds to the photoelectron emission from the $Zr3d_{5/2}$ and $Zr3d_{3/2}$ energy states characteristics of Zr(IV) species in oxide environment [36,43]. The C1s region a board and intense XPS peak was observed at 284.6 eV along with a broad intense shoulder at 289.7 eV. The former peak is assigned to the adventitious carbon whereas the high binding energy peak is due to the presence of a minor amount of carbonate species on the surface of the composite [44]. The O1s high resolution spectrum is broad and complicated due to the overlapping contribution from different types of oxygen species present in the sample. The broad spectrum can be deconvoluted into three regions with binding energy maxima at 529.8, 531.2 and 532.2 eV. These peaks can be assigned to the lattice oxygen of the $Ca_xZr_{1-x}O_{2-x}$ solid solution phase and oxygen from CaO and surface carbonate species. Pure CaO and $Ca(OH)_2$ is known to exhibit O 1s peak ~ 531.2- 531.6 eV whereas for $CaCO_3$ the O1s peak occur at 532.5 eV [45]. For pure ZrO_2 the lattice oxygen binding energy appears at 530.1 eV [36]. It has been observed that when Zr^{4+} ions are doped into the CaO lattice the O1s peak shifts progressively to lower binding energy. Hence assigning the lower binding energy peak to the solid solution phase is in line with the literature report [43]. In this study, neither the formation of cubic $CaZrO_3$ phase nor the crystalline CaO phase was detected in XRD study of 20Ca-Zr-O. It is likely that the 20Ca-Zr-O sample may contain a small portion of Ca^{2+} ions as amorphous CaO/$Ca(OH)_2$ phase which escaped XRD detection. These species are responsible for the peak at 531.2 eV. In the Ca2p high resolution spectra, the prominent peak at 346.1 eV along with a satellite at 350.6 eV corresponds to the photoelectron emission from the

Ca2p3/2 and Ca2p1/2 states. These peaks are characteristics of Ca^{2+} ions in oxide environment [43-47]. However, unlike pure CaO, where a well-defined valley is observed between the two peaks, in this study these two peaks are broad and unresolved from one another. This may be due to the fact that a small fraction of Ca^{2+} may exist in carbonate environment [44,45]. The $CaCO_3$ show Ca2p doublet at 347.4 and 351.0 eV. The presence of Ca^{2+} ions in the solid solution phase and a small fraction as surface carbonate species can be inferred from the XPS study.

The Raman spectra of the xCa-Zr-O composite materials along with pure ZrO_2 are presented in Fig. 6. The Raman technique is an effective method for microstructural analysis of crystalline oxide phases. Particularly, the Raman technique has been highly effective for characterization of different polymorphic forms of zirconia in composite materials [22,48, 49]. Pure ZrO_2 prepared by urea hydrolysis method exhibit intense Raman bands with maxima at 177, 187, 220, 331, 381, 500, 536, 559 and 615 cm^{-1} corresponding to the monoclinic phase and 146, 269,314, 475 and 638 cm^{-1}corresponding to the tetragonal phase of zirconia [22, 49]. In contrast to this observation, the xCa-Zr-O composite oxide exhibit broad, asymmetric and low intense Raman bands corresponding to the t-ZrO_2 only [16,22]. The broadening of the peaks may be ascribed to the presence of large amount of oxygen vacancy created due to incorporation of Ca^{2+} ions into the ZrO_2 lattice [16,22]. Tetragonal zirconia belongs to $P4_2$/nmc space group and is expected to exhibit six Raman active vibration modes having $A_{1g} + 3E_g + 2B_{1g}$ symmetry [48,49]. Among these vibrational modes, the symmetric A_{1g} vibration appears around 600 cm^{-1} and is often too weak to be observed. In the present study for the xCa-Zr-O composite, the broad Raman bands observed at 146 and 318 cm^{-1} can be assigned to 2 B1g modes and the bands at 269, 456 and 642 $cm^{-1}$to the 3Eg modes, respectively. The asymmetric nature of the Raman bands indicates distortion in the oxygen sub-lattice caused by the insertion of the Ca^{2+} ions into the zirconia lattice.

The surface basic property of the xCa-Zr-O composite materials was studied using the CO_2-TPD technique. The TPD profiles of the xCa-Zr-O composite materials are presented in Fig.7. The TPD profiles for the composite oxides contain three CO_2 desorption regions in the temperature range of < 400 K, 450-750 K and >750 K. Pure ZrO_2 prepared by urea hydrolysis method exhibit significant CO_2 desorption below 400 K (Fig. 7a). This low temperature TPD peak can be assigned to the presence of weak basic sites on zirconia surface. The addition of Ca^{2+} ions into the zirconia lattice improves the CO_2 retention at high temperature indicating generation of new basic sites of higher strength (Fig. 7 b-e). For the 5Ca-Zr-O, 10Ca-Zr-O and 20Ca-Zr-O materials a strong CO_2 desorption peak is noticed in the range of 400-750 K. Simultaneously, the low temperature desorption peak below 400 K is significantly suppressed. With increase in Ca^{2+} content in the composite, the high temperature TPD peak progressively shifts towards the higher temperature side. For 50Ca-Zr-O material, a single prominent desorption peak is observed with peak maxima at 790 K (Fig, 7e). The CO_2-TPD method has been used earlier for characterization of basic sites of CaO-ZrO_2 composite materials. The basicity of the CaO-ZrO_2 material depends on various factors such as the preparation method, the crystallographic phase of zirconia, CaO content and calcinations temperature [11, 15-18, 22]. The tetragonal phase of zirconia and a higher calcination temperature facilitates the incorporation of Ca^{2+} ions into the zirconia lattice [18,22]. The presence of Ca^{2+} ions in the vicinity of O^{2-} ions improves the basicity of the lattice oxygen on the surface. Moreover, the incorporation of Ca^{2+} to ZrO_2 lattice leads to the formation of Ca-O-Zr linkages and uneven charge distribution which is responsible for generation of new basic sites [13]. In the present study, the desorption peak in the temperature range of 450-750 K can be assigned to the generation of new basic sites due to solid solution formation. The TPD peak observed at 790 K for 50Ca-Zr-O material can be ascribed to the formation of CaO crystallites which has been detected in XRD study for this sample. At high CaO content, the CaO crystallites segregates along the grain boundary area which is responsible for the high temperature CO_2 desorption [18]. Table 1 provides a summary of the number of basic sites observed for the composite materials. The number of basic sites increases with CaO content upto 20 mol% beyond which there is a marginal decrease for 50Ca-Zr-O material. The TPD study clearly indicates that the CaO-ZrO_2 composite materials contain strong surface basic sites. The specific surface area of the Ca-Zr-O composite materials is presented in Table 1. Pure ZrO_2 prepared by urea hydrolysis method exhibit specific surface area of 58.2 m^2/g. In general, the nanocomposite oxides exhibit higher surface area compared to the pure zirconia material. Highest surface area of 91.2 m^2/g is obtained for the 20Ca-Zr-O material. The Ca-Zr-O composite oxides prepared by urea hydrolysis method exhibit more number of strong basic sites (450-750 K) and higher surface area compared to CaO-ZrO_2 materials prepared by impregnation, coprecipitation, birch-templating and combustion synthesis methods [11,14,15,18,20]. The urea hydrolysis method seems to be effective for synthesis of high surface area Ca-Zr-O composite oxides with strong surface basicity. Urea is a weak Bronsted base (pK_b=13.8) whose hydrolysis rate can be controlled by varying the temperature [50]. The mild nature of urea is helpful in terms of controlled hydrolysis and precipitation of the metal cations resulting in materials with high surface area. The slow hydrolysis rate also ensures uniform precipitation of the two components leading to compositional homogeneity and formation of a uniform solid solution (as evident from elemental mapping study in HRTEM). These factors contribute to the high surface area and basicity of Ca-Zr-O composite samples prepared by urea hydrolysis method.

The FESEM images of the xCa-Zr-O material are presented in Fig. 8. Pure ZrO_2 prepared by urea hydrolysis method contain submicron size elongated rod like particles (Fig. 8a). Upon incorporation of Ca^{2+} into zirconia lattice morphological changes are clearly noticed in the FESEM study. The 5Ca-Zr-O and 10Ca-Zr-O materials contain agglomerated particles of irregular shape with size in the submicron range (Fig. 8b and 8c). With further increase in CaO content the appearance of flake like particles is observed for 20Ca-Zr-O and 50Ca-Zr-O materials (Fig. 8d and 8e). The flake like particles are formed by controlled growth along the X and Y planar direction. The pure CaO, on the other hand, contain particles with distinct cubic morphology (Fig. 8f). Considerable intergrowth among the cubic particles is noticed from the FESEM study. The TEM image of the 20Ca-Zr-O material along with the EDX pattern and elemental mapping analysis is presented in Fig. 9. The presence of flake like nanostructures can be inferred from the TEM study (Fig. 9a). The high resolution image of the 20Ca-Zr-O material indicate the presence of quasi spherical particles with size in the range of 5-11 nm attached to each other through the grain boundary region (Fig. 9b). The Fourier analysis data is found to be complementing the TEM observation. The EDX pattern of the 20Ca-Zr-O material is presented in Fig. 9c. The presence of Ca, Zr and O of required stoichiometry is inferred from the EDX analysis. The elemental mapping analysis images of the 20Ca-Zr-O composite materials are presented in Figs 9d-g. Uniform distribution of both Ca^{2+} and Zr^{4+} ions through the specimen sample can be noticed from the elemental mapping study.

<H2>3.2 Catalytic application of the xCa-Zr-O nanocomposite oxides for base catalyzed synthesis of chromene analogues

The catalytic activity of the xCa-Zr-O composite oxides is evaluated for the base catalyzed one pot multicomponent synthesis of 2-amino 4H-Chromenes and 2-amino-2-chromenes. The 2-amino-5-

oxo-5,6,7,8-tetrahydro-4H-chromenes were synthesized by one pot condensation of aryl aldehydes, dimedone and malononitrile (Scheme 1). Initially, the condensation of benzaldehyde, dimedone and malononitrile was taken as a model reaction and xCa-Zr-O materials with different composition were evaluated as heterogeneous base catalyst at 50^{o}C employing aqueous ethanol (1:1) as reaction media. The results of these catalytic experiments are presented in Table 2. Pure zirconia prepared by urea hydrolysis method provided an isolated yield of 32.6% after 3h of reaction time. The weak basic sites of zirconia are ineffective in expediting the base catalyzed the multicomponent reaction. Addition of CaO into the zirconia matrix improves the yield of the 4H-chromene simultaneously reducing the reaction time. Best catalytic results were obtained when 20Ca-Zr-O composite oxide was used as heterogeneous base catalyst (Table 2). The 20Ca-Zr-O material provides an isolated yield of 82.6% within 1 h of reaction time. The catalytic results presented in Table 2 are well correlated with the basicity data presented in Table 1. As observed from the TPD study, the incorporation of Ca^{2+} ions into zirconia creates new basic sites simultaneously modulating the basicity of the oxygen sublattice. The enhancement in basicity is responsible for the improved catalytic performance of the Ca-Zr-O composite oxides for 4H-chromene synthesis. Since the composite oxide materials exhibit different surface area and basicity, in order to compare their catalytic performance, the reaction rates are calculated by estimating the benzaldehyde conversion in the reaction mixture using gas chromatography. The rate of reaction with respect to unit surface area and mass is presented in Table 2. Among all Ca-Zr-O composite oxide materials, the 20Ca-Zr-O material exhibit highest reaction rate indicating its superior performance for the base catalyzed reaction. For the sake of comparison, the 20Ca-Zr-O material is also prepared by co-precipitation (P) method using liquid ammonia as precipitating agent and impregnation (I) method. The 20Ca-Zr-O material prepared by urea hydrolysis method displays higher reaction rate per unit surface and provides better isolated yield of the 2-amino 4H-chromene compared to the 20Ca-Zr-O-I and 20Ca-Zr-O-P materials. The reaction rate per unit surface depends on the preparation method (Table 2). Structurally, the 20Ca-Zr-O composite materials prepared by urea hydrolysis and coprecipitation methods contain a solid solution phase whereas the 20Ca-Zr-O-I material contains a mixture of monoclinic and tetragonal zirconia phase along with crystalline $CaO/Ca(OH)_2$ phases (Fig. S1). The urea hydrolysis method is particularly useful for preparation of composite oxides with compositional homogeneity, higher surface area and basicity. In order to compare the catalytic activity of the 20Ca-Zr-O catalyst with other zirconia based alkali and alkaline earth composite oxides, 20M-Zr-O (where M = Ba and Mg) materials are prepared by urea hydrolysis method. The catalytic activity of the 20M-Zr-O catalyst varies in the order 20Ca-Zr-O > 20Mg-Zr-O > 20Ba-Zr-O (Table 2). Based on the catalytic activity data presented in Table 2, the 20Ca-Zr-O composite oxide material is chosen for further catalytic study. In order to optimize the reaction protocol, the base catalyzed reaction us performed by varying the catalyst weight, temperature and reaction media. The results of these optimization experiments are presented in Fig. 10. For reaction involving 2 mmol of the reactants, 50 mg of the catalyst is ideal for efficient condensation of the three components (Fig. 10I). Further increase in catalyst weight does not have a marked impact on the yield of the product. Similarly, the yield of the product increases with increase in temperature before attending saturation at 50^{o}C (Fig. 10II). After optimizing the catalyst weight and temperature, we used different solvents to study the effect of reaction media on the base catalyzed condensation reaction. The condensation reaction is expedited in presence of polar solvent. Among different polar solvent used ethanol provide better yield of the product. The poor yield observed in case of water is attributed to the limited solubility and poor accessibility of the reactants to the catalyst surface. The best results were obtained when a mixed solvent system comprising of ethanol and water (1:1 molar ratio) is used (Fig. 10III). After optimizing the reaction conditions, we explored the scope and limitation of the developed catalytic method, by using different substituted aldehydes in the optimized protocol (Table 3). The yield of the 4H-chromene is found to be marginally better in case of aromatic aldehydes containing electron withdrawing groups. However, a variety of aromatic aldehydes reacted efficiently under the optimized catalytic conditions to provide the corresponding 4H-chromenes in high yield and purity.

Encouraged by the results of the catalytic experiments, we further studied the applicability of xCa-Zr-O composite oxide materials as heterogeneous base catalyst for synthesis of 2-amino-2-chromenes by one pot condensation of α-naphthol, aryl aldehydes and malononitrile (Scheme 1). Initially, the reaction conditions are optimized by taking the condensation of benzaldehyde, α-naphthol and malononitrile as a model reaction. It is observed that for a reaction involving 2 mmol of reactants, 50 mg of the catalyst is sufficient for the condensation of the three components. The condensation reaction is carried out in different solvents. Table 4 provides a comparison of the catalytic activity of the composite materials with Ca based catalysts in different reaction media. Among different solvents studied for the reaction, the polar solvents provide better yield of the product compared to nonpolar solvents. Among different polar solvents studied at 50^{o}C, best results are obtained when a mixture of PEG and water (1:1) is used. For solvents like water, chloroform and ethanol, the formation of the 2-amino-2-chromenes require longer time with poor yield of the product at 50^{o}C. When the reaction is carried out under reflux condition, the product yield is found to improve for these solvents (Table 4). The use of this mixed solvent system considerable reduces the reaction temperature and time. Among the composite oxide, the 20Ca-Zr-O material is catalytically more active compared to 10Ca-Zr-O, CaO and $CaCO_3$ which is mainly ascribed to the enhanced basicity of this composite oxide. In order to confirm that the reaction is truly heterogeneous in nature, the concentration Ca^{2+} ions in the used solvent was measured using atomic absorption spectroscopy (AAS). No appreciable concentration of Ca^{2+} ions could be detected in the used solvent indicating that the leaching of the Ca^{2+} does not takes place during the reaction. The stability of the Ca^{2+} ions in the Ca-Zr-O catalyst could be ascribed to the formation of the solid solution phase as a result of incorporation of Ca^{2+} ions into the zirconia lattice. After optimizing the reaction conditions, the applicability of the 20Ca-Zr-O catalyzed multicomponent condensation protocol is extended to the synthesis of structurally diverse 2-amino2-chromenes by using different substituted aryl aldehydes (Table 5). Under identical reaction conditions, aryl aldehydes bearing electron withdrawing and donating groups reacted efficiently to give the corresponding 2-amino-2-chromenes in high yield and purity. The recyclability of the 20Ca-Zr-O catalyst is tested for three consecutive cycles for synthesis of 2-amino-2-chromene. After completion of each cycle, the catalyst particles are filtered, washed with excess of water and later with 05 ml of ethanol and dried in hot air oven. The catalyst particles are regenerated by heat treatment at 500^{o}C for 2 h. The 20Ca-Zr-O catalyst retains its catalytic activity upto three cycles without any significant decrease in yield of the product (Table 5, Entry 1, yields, 88.6%, 1st; 87%, 2nd; 85%, 3rd). The recyclability test indicates stable activity of the 20Ca-Zr-O material for synthesis of 2-amino2-chromenes. The heterogeneous catalytic protocol developed in this work offer distinct advantage in terms of easy recovery and recyclability of the catalyst compared to many literature reported homogeneous catalyst methods such as the piperazine, Potassium phthalimide, CTACl, triethyl amine, tetrabutylammonium fluoride, I_2/K_2CO_3, basic ionic liquid, acid hydrolysate of tendons [24, 25,29-31, 33-35]. Moreover, although the yield obtained in this method are comparable with the earlier methods, the present protocol is advantageous in terms of the use of lower catalyst amount, low reaction temperature (in many studies reflux condition and aqueous media has been used) and use of mixed solvent system.

A plausible mechanism for synthesis of the chromene analogues over the xCa-Zr-O composites is presented in scheme 2. Initially, the Knoevenagel condensation reaction between the aryl aldehyde with malononitrile leads to the formation of arylidenemalononitrile. The basic sites of the xCa-Zr-O catalyst can activate the malononitrile to promote the Knoevenagel condensation. The nucleophilic addition of the enolic form of the dimedone to arylidenemalononitrile affords the intermediate I. The formation of the enolic form of the dimedone can be facilitated on the O^{2-} basic sites on the catalyst surface. The intermediate I is subsequently cyclized by nucleophilic attack of the OH group on the CN moiety, which undergo tutomerization to provide the 2-amino 4H chromenes. Similarly, during synthesis of 2-amino-2-chromene, the ortho C-alkylation of α-naphthol takes place by reaction with arylidenemalononitrile to give the intermediate II. The ortho C-alkylation is favored in presence of xCa-Zr-O catalyst due to the perpendicular adsorption of the α-naphthol molecule over the catalyst surface. It has been observed that the heterogeneous base catalysts are highly selective to ortho alkylation of phenol moieties. The phenolic molecules adsorb perpendicularly to the catalyst surface to minimize the repulsion between electron rich surface sites and the aromatic ring [51]. The intermediate II reacts in a similar fashion as that of intermediate I by following the nucleophilic addition and tutomeriztion steps on the xCa-Zr-O surface to produce the 2-amino-chromenes.

<H1>4. Conclusion

In this study, we have prepared a series of CaO-ZrO_2 nanocomposite oxides and explored their catalytic application for synthesis of chromene analogues. The urea hydrolysis method provided well dispersed CaO-ZrO_2 composite oxide materials with compositional homogeneity. The incorporation of Ca^{2+} ions into the zirconia lattice leads to the formation of an oxygen deficient solid solution phase which retains the tetragonal crystal structure of zirconia. Upto 20 mol% CaO content in the composite oxide a homogeneous solid solution phase is formed whereas the formation of a mixed phase system is noticed beyond 20 mol%. Fourier and TEM analysis indicated formation of nanocrystallites of the composite oxide with size less than 20 nm. The generation of new basic sites of higher strength due to the presence of Ca^{2+} ions in ZrO_2 lattice could be inferred from the TPD study. XPS study indicated the presence of different lattice oxygen as potential basic sites. The morphological reorganization of the particles with increase in CaO content is inferred from FESEM study. The CaO-ZrO_2 nanocomposite oxides exhibit excellent catalytic activity for synthesis of chromene analogues. Structurally diverse 2-amino-2-chromenes and 2-amino-4H-Chromenes were synthesized under mild condition using the xCa-Zr-O composite materials as catalyst. The heterogeneous catalytic protocol developed in this work is advantageous in terms of simple experimentation, use of recyclable catalyst, mild reaction condition and high yield and purity of the products.

Acknowledgement

We would like to thank the Board of Research in Nuclear Sciences (BRNS), Mumbai for financial support through the grant No. 37(2)/14/23/2015/BRNS.

<REF>References

<BIBL>
[1] Y. Ono, H. Hattori,;1; Solid Base Catalysis, 2012, <PN>Springer Verlag</PN>, <PL>Berlin, Germany</PL>.

[2] G. Busca,;1; Chem. Rev. 110 (2010) 2217–2249.

[3] A.F. Lee, J.A. Bennett, J.C. Manayil, K.Wilson,;1; Chem. Soc. Rev. 43(2014) 7887–7916.

[4] D. Kumar,V.B. Reddy,B.G. Mishra,R.K. Rana,M.N. Nadagouda, R.S. Varma,;1; Tetrahedron 63 (2007) 3093–3097.

[5] S. Samantaray, D.K. Pradhan, G. Hota, B.G. Mishra,;1; Chem. Eng. J. 193 (2012) 1–9.

[6] L.B. Sun, X.Q. Liu, H.C. Zhou,;1; Chem. Soc. Rev. 44 (2015) 5092–5147.

[7] B. Hamad, A. Perard, F. Figueras, S. Prakash, N. Essayem,;1; J. Catal. 269 (2010) 1–4.

[8] L. Gong, L. Sun, Y. Sun, T. Li, X. Liu,;1; J. Phys. Chem. C 115 (2011) 11633–11640.

[9] X. Tian, Y. Zeng, T. Xiao, C. Yang, Y. Wang, S. Zhang,;1; Micropor. Mesopor. Mater. 143 (2011) 357–361.

[10] W. Shen, G.A. Tompsett, K.D. Hammond, R. Xing, F. Dogan, C.P. Grey, W.C. Conner Jr, S.M. Auerbach, G.W. Hube,;1; Appl. Catal. A. Gen. 392 (2011) 57–68.

[11] H. Duan, Y. Yamada, S. Sato,;1; Appl. Catal. A. Gen. 487 (2014) 226–233.

[12] C. Wang, N. Sun, M. Kang, X. Wen, N. Zhao, F. Xiao, W. Wei, T. Zhao, Y. Sun,;1; Catal. Sci. Technol. 3 (2013) 2435–2443.

[13] S. Liu, J. Ma, L. Guan, J. Li, W. Wei, Y. Sun,;1; Micropor. Mesopor. Mater. 117 (2009) 466–471.

[14] L. Liu, Z. Wen,;1; Fuel 158 (2015) 176–182.

[15] H. Wang, M. Wang, S. Liu, N. Zhao, W. Wei, Y. Sun,;1; J. Mol. Catal. A: Chem. 258 (2006) 308–312.

[16] X. Tian, T. Xiao, C. Yang, Z. Zhou, H. Ke,;1; Mater. Chem. Phys. 124 (2010) 744–747.

[17] S. Xia, X. Guo, D. Mao, Z. Shi, G. Wu, G. Lu,;1; RSC Adv. 4 (2014) 51688–51695.

[18] H. Wang, M. Wang, W. Zhang, N. Zhao, W. Wei, Y. Sun,;1; Catal. Today 115 (2006) 107–110.

[19] Q.J. Chen, J. Zhang, Q.W. Jin, B.R. Pan, W.B. Kong, T.J. Zhao, Y.H. Sun,;1; Catal. Today 215 (2013) 251– 259.

[20] H. Zhao, M. Lin, K. Fang, J. Zhou, Z. Liu, G. Zeng,Y. Sun,;1; RSC Adv. 5 (2015) 67630–67637.

[21] V. Nichelea, M. Signorettoa, F. Pinnaa, F. Menegazzoa, I. Rossettib, G. Crucianic, G. Cerratod, A.D. Michelee,;1; Appl. Catal. B. Env. 150 (2014) 12– 20.

[22] T.Y. eda, S. Kitamura, N.O. Ikenaga, T. Miyake, T. Suzuki,;1; J. Mol. Catal. A: Chem. 323 (2010) 7–15.

[23] N. Majumdar,N.D. Paul,S. Mandal,B.de Bruin,W.D. Wulff,;1; ACS Catal. 5 (2015) 2329−2366.

[24] K. Gong, H.L. Wang, D. Fang, Z.L. Liu,;1; Catal. Commun. 9 (2008) 650–653.

[25] Y. M. Ren, C. Cai,;1; Catal. Commun. 9 (2008) 1017–1020.

[26] K. Niknam, N. Borazjani, R. Rashidian, A. Jamali,;1; Chin. J. Catal. 34 (2013) 2245–2254.

[27] D. Kumar, V.B. Reddy, S. Sharad, U. Dube, S. Kapur,;1; Eur. J. Med. Chem. 44 (2009) 3805–3809.

[28] V. M. Joshi, R. L. Magar, P.B. Throat, S.U. Tekale, B.R. Patil, M.P. Kale, R.P. Pawar,;1; Chin. Chem. Lett. 25 (2014) 455–458.

[29] R. Ballini, G. Bosica, M.L. Conforti, R. Maggi, A. Mazzacani, P. Righic, G. Sartori,;1; Tetrahedron 57 (2001) 1395-1398.

[30] J. Banothu, R. Velpula, R. Gali, R. Bavantula, P.A. Crooks,;1; Tetrahedron Lett. 54 (2013) 3862–3864.

[31] Y. Zhen, H. Lin, S. Wanga, M. Tao,;1; RSC Adv. 4 (2014) 26122–26128.

[32] R. Sangsuwan, S. Sangher, T. Aree, C. Mahidol, S. Ruchirawat, P. Kittakoop,;1; RSC Adv. 4 (2014) 13708–13718.

[33] S. Gao, C.H. Tsai, C. Tseng, C.F. Yao,;1; Tetrahedron 64 (2008) 9143–9149.

[34] M. Amirnejad, M.R. Naimi-Jamal,;1; Monatsh. Chem. 144 (2013) 1219–1225.

[35] H. Kiyani, F. Ghorbani,;1; J. Saudi Chem. Soc.18 (2014) 689–701.

[36] S. Pradhan, B.G. Mishra,;1; RSC Adv. 5 (2015) 86179–86190.

[37] S. Samantaray, P. Kar, G. Hota, B.G. Mishra,;1; Ind. Eng. Chem. Res. 52 (2013) 5862−5870.

[38] S. Samantaray, B.G. Mishra,;1; J. Mol. Catal. A: Chem. 339 (2011) 92–98.

[39] L. Chen, J. Hu, R.M. Richards,;1; Chem. Phys. Chem. 9 (2008) 1069 – 1078.

[40] S. Figueroa, J. Desimoni, P.C. Rivas, M.M. Cervera, M.C. Caracoche,;1; Chem. Mater. 17 (2005) 3486 –3491.

[41] B.E. Warren, B.L. Averbach,;1; J. Appl. Phys. 21 (1950) 595.

[42] D. Balzar, H. Ledbetter,;1; J. Appl. Cryst. 26 (1993) 97 –103.

[43] R. Koirala, K.R. Gunugunuri, S.E. Pratsinis, P.G. Smirniotis,;1; J. Phys. Chem.C 115 (2011) 24804–24812.

[44] M.L. Granados,M.D.Z. Poves,D.M. Alonso,R. Mariscal,F.C. Galisteo,R.M. Tost, J. Santamarıa, J.L.G. Fierro,;1; Appl.Catal. B. Environ. 73 (2007) 317–326.

[45] M.I. Sosulnikov, Y.A. Teterin,;1; J. Electron. Spectrosc. Relat. Phenom. 69 (1992) 111 –126.

[46] S.L. Martínez, R. Romero, J.C. Lopez, A. Romero, V.S. Mendieta, R. Natividad,;1; Ind. Eng. Chem. Res. 50 (2011) 2665–2670.

[47] X.Y. Qiu, H.W. Liu, F. Fang, M.J. ha, X.H. Zhou, J.M. Liu,;1; Appl. Phys. A. 81 (2005) 1431–1434.

[48] D. Spielbauer, G.A.H. Mekhemer, E. Bosch, H. Knozinger,;1; Catal. Lett. 36 (1996) 59–68.

[49] L. Shi, K.C. Tin, N.B. Wong,;1; J. Mater. Sci. 34 (1999) 3367 – 3374.

[50] U. Costantino, F. Marmottini, M. Nocchetti, R. Vivani,;1; Eur. J. Inorg. Chem. (1998) 1439-1446.

[51] S. Sato, K. Koizumi, F. Nozaki,;1; J. Catal. 178 (1998) 264.

</BIBL>

<Figure>Fig. **1.** X-ray diffraction patterns of (a) ZrO_2, (b) 2Ca-Zr-O, (c) 5Ca-Zr-O, (d) 10Ca-Zr-O, (e) 20Ca-Zr-O and (f) 50Ca-Zr-O materials.

<Figure>Fig. **2.** (I)XRD patterns indicating an gradual shift in the peak position of TZ (111) peak to lower 2θ value with CaO content (a) ZrO_2, (b) 2Ca-Zr-O, (c) 5Ca-Zr-O, (d) 10Ca-Zr-O, (e) 20Ca-Zr-O and (f) 50Ca-Zr-O, (II) variation of cell volume with CaO content for the xCa-Zr-O nanocomposite materials.

<Figure>Fig. **3.** Fourier line profile plots for the ZrO_2 and Ca-Zr-O nanocomposite material.

<Figure>Fig. **4.** TG profiles of 10Ca-Zr-O (panel I) and 50Ca-Zr-O (panel II) along with the DSC profiles (a) 10Ca-Zr-O and 50Ca-Zr-O (panel III).

<Figure>Fig. **5.** XPS spectra of 20Ca-Zr-O material.

<Figure>Fig. **6**. Raman Spectra of (a) ZrO_2, (b) 5Ca-Zr-O, (c) 10Ca-Zr-O and (d) 20Ca-Zr-O.

<Figure>Fig. **7.** CO_2 TPD profiles of (a) ZrO_2, (b) 5Ca-Zr-O, (c) 10Ca-Zr-O, (d) 20Ca-Zr-O and (e) 50Ca-Zr-O materials.

<Figure>Fig. **8.** FESEM images of (a) ZrO_2, (b) 5Ca-Zr-O, (c) 10Ca-Zr-O, (d) 20Ca-Zr-O, (e) 50Ca-Zr-O and (f) CaO.

<Figure>Fig. **9.** TEM images (a, b), EDX pattern (c) and elemental analysis study (d-g) of 20Ca-Zr-O material.

<Figure>Fig. **10.** Effect of reaction parameters on yield of the model reaction. (I) Effect of catalyst amount (aqueous ethanol (1:1), 50°C), (II) effect of temperature (aqueous ethanol (1:1), 50 mg catalyst) and (III) effect reaction media (50 mg catalyst, 50°C).

Material	**Specific surface area (m^2/g)**	**Crystallite size[a] (nm)**	**Strain $<e^2>^{1/2}$**	**CO_2 desorption (mmol/g)**			**Total Basicity[b] (mmol/g)**
				< 400 K	450-750 K	> 750 K	
ZrO_2	58.2	16.9	4.82×10^{-3}	0.104	---	---	0.104
5Ca-Zr-O	68.9	7.5	2.16×10^{-3}	---	0.230	---	0.230
10Ca-Zr-O	82.6	11.4	3.46×10^{-3}	---	0.370	--	0.370
20Ca-Zr-O	91.2	13.5	3.93×10^{-3}	---	0.418	0.220	0.630
50Ca-Zr-O	68.6	20.4	5.47×10^{-3}	---	0.075	0.485	0.560

<Figure>**Scheme 1.** Synthesis of chromene analogues catalyzed by xCa-Zr-O composite materials.

<Figure>**Scheme 2**. Plausible mechanism for synthesis of chromene analogues over the xCa-Zr-O catalyst

<Table>Table 1**.** Physicochemical Characteristics of xCa-Zr-O composite materials.

a. *Calculated form Fourier line profile of broadened XRD profile,* ***b.*** *Calculated from CO_2 TPD profile*

<Table>Table 2**.** Catalytic activity of xCa-Zr-O materials towards the synthesis of 4H-chromenes.

Catalyst	**Time (min)**	**Yield[a,b]**	**Reaction rate[c] ($mmolh^{-1}g^{-1}$)**	**Reaction rate ($mmolh^{-1}m^{-2} \times 10^{-3}$)**
ZrO_2	180	32.6	4.6	2.0
5Ca-Zr-O	90	55.8	15.6	6.7
10Ca-Zr-O	60	65.2	27.0	8.1
20Ca-Zr-O	60	82.6	33.8	9.4
50Ca-Zr-O	90	73.3	20.0	7.3
20Ca-Zr-O-P	90	71.6	19.4	7.1
20Ca-Zr-O-I	120	65.8	13.6	6.8
20Mg-Zr-O	90	76.5	20.8	--
20Ba-Zr-O	120	45.3	9.4	--

a. *Reaction conditions: benzaldehyde (2mmol), malononitrile (2 mmol), dimedone (2 mmol) and 50 mg catalyst in 3 ml of aqueous ethanol (1:1 ratio) at 50°C for 1 h,* ***b.*** *Refer to pure and isolated yield,* ***c.*** *Calculated with respect to the benzaldehyde conversion in the reaction mixture analyzed using gas chromatography*

<Table>Table 3**.** 20Ca-Zr-O catalyzed synthesis of structurally diverse 4H-chromenes.

Sl No	**R**	**Time (min)**	**Yield[a] (%)**
1	H	60	82.6
2	4-NO_2	60	90.2
3	4-Cl	60	88.5
4	4-OCH_3	90	83.2
5	3-NO_2	60	87.3
6	4-Br	90	85.4
7	4-OH	90	81.6
8	4-Me	90	76.5
9	2-NO_2	60	91.8
10	4-F	60	82.1

a. *Reaction conditions: aryl aldehydes (2 mmol), malononitrile (2 mmol), dimedone (2 mmol) and 50 mg of 20Ca-Zr-O catalyst in 3 ml of aqueous ethanol (1:1 ratio) at 50°C*

<Table>Table 4**.** Catalytic activity of Ca-Zr-O materials towards the synthesis of 2-amino-2-chromenes.

Solvent	**Catalyst**	**Temperature**	**Time (min)**	**Yield[a,b] (%)**
Ethanol	20Ca-Zr-O	50°C	180	59.6
Chloroform	20Ca-Zr-O	50°C	180	42.2
Water	20Ca-Zr-O	50°C	180	51.5
PEG + Water (1:1)	20Ca-Zr-O	50°C	60	88.6
PEG + Water (1:1)	10Ca-Zr-O	50°C	60	73.5
PEG + Water (1:1)	$CaCO_3$	50°C	60	65.1
PEG + Water (1:1)	CaO	50°C	60	78.2
Ethanol	20Ca-Zr-O	reflux	90	84.0
Chloroform	20Ca-Zr-O	reflux	90	76.8
Water	20Ca-Zr-O	reflux	60	80.5

a. *Reaction conditions: benzaldehyde (2 mmol), malononitrile (2 mmol), α-naphthol (2 mmol) and 50 mg of catalyst in 3 ml of solvent,* ***b.*** *Refer to pure and isolated yield*

<Table>Table 5**.** 20Ca-Zr-O catalyzed synthesis of structurally diverse 2-amino-2-chromenes.

Sl No	**R**	**Time (min)**	**Yield[a] (%)**
1	H	60	88.6
2	2-NO_2	60	89.5
3	4-NO_2	60	91.2
4	4-OCH_3	90	83.6
5	2-Cl	60	87.0
6	3-NO_2	90	84.5
7	4-Cl	60	90.4
8	4-Br	90	80.5
9	4-F	120	82.5

10	4-CH_3	120	81.0

a. *Reaction conditions: 2 mmol of reactants with molar ratio 1:1:1, 50 mg of 20Ca-Zr-O catalyst, 3 ml of PEG–water (3 ml; 1:1 mixture) as solvent, temperature 50^{o}C,* ***b.*** *Refer to pure and isolated yield*

TDENDOFDOCTD